Biomedical Optics EXPRESS

Optical coherence tomography-based freeze-drying microscopy

Mircea Mujat,[1,*] Kristyn Greco,[2] Kristin L. Galbally-Kinney,[1] Daniel X. Hammer,[1] R. Daniel Ferguson,[1] Nicusor Iftimia,[1] Phillip Mulhall,[1] Puneet Sharma,[2] Michael J. Pikal,[2] and William J. Kessler [1]

[1]*Physical Sciences, Inc., 20 New England Business Center, Andover, MA 01810, USA*
[2]*School of Pharmacy, University of Connecticut, 69 North Eagleville Road, Storrs, CT 06269, USA*
**mujat@psicorp.com*

Abstract: A new type of freeze-drying microscope based upon time-domain optical coherence tomography is presented here (OCT-FDM). The microscope allows for real-time, *in situ* 3D imaging of pharmaceutical formulations in vials relevant for manufacturing processes with a lateral resolution of <7 μm and an axial resolution of <5 μm. Correlation of volumetric structural imaging with product temperature measured during the freeze-drying cycle allowed investigation of structural changes in the product and determination of the temperature at which the freeze-dried cake collapses. This critical temperature is the most important parameter in designing freeze-drying processes of pharmaceutical products.

©2011 Optical Society of America

OCIS codes: (110.0180) Microscopy; (110.4500) Optical coherence tomography; (180.6900) Three-dimensional microscopy.

References and links

1. C. Arnst, A. Weintraub, J. Carey, K. Capell, and M. Arndt, "Biotech, finally," in Business Week, June 13, 2005, issue 3937, http://www.businessweek.com/magazine/content/05_24/b3937001_mz001.htm.
2. M. J. Pikal and S. Shah, "The collapse temperature in freeze drying: dependence on measurement methodology and rate of water removal from the glassy phase," Int. J. Pharm. **62**(2-3), 165–186 (1990).
3. X. Tang and M. J. Pikal, "Design of freeze-drying processes for pharmaceuticals: practical advice," Pharm. Res. **21**(2), 191–200 (2004).
4. E. Meister and H. Gieseler, "Freeze-dry microscopy of protein/sugar mixtures: drying behavior, interpretation of collapse temperatures and a comparison to corresponding glass transition data," J. Pharm. Sci. **98**(9), 3072–3087 (2009).
5. D. Huang, E. A. Swanson, C. P. Lin, J. S. Schuman, W. G. Stinson, W. Chang, M. R. Hee, T. Flotte, K. Gregory, C. A. Puliafito, and J. G. Fujimoto, "Optical coherence tomography," Science **254**(5035), 1178–1181 (1991).
6. A. F. Fercher, W. Drexler, C. K. Hitzenberger, and T. Lasser, "Optical coherence tomography - principles and applications," Rep. Prog. Phys. **66**(2), 239–303 (2003).
7. K. Kobayashi, J. A. Izatt, M. D. Kulkarni, J. Willis, and M. V. Sivak, Jr., "High-resolution cross-sectional imaging of the gastrointestinal tract using optical coherence tomography: preliminary results," Gastrointest. Endosc. **47**(6), 515–523 (1998).
8. B. D. Mac Neill, H. C. Lowe, E. Pomeranstev, D. DeJoseph, H. Yabushita, G. J. Tearney, B. E. Bouma, and I. K. Jang, "In-vivo characterization of plaque morphology by optical coherence tomography predicts coronary artery remodeling," J. Am. Coll. Cardiol. **41**(6), 42 (2003).
9. S. H. Yun, G. J. Tearney, J. F. de Boer, N. Iftimia, and B. E. Bouma, "High-speed optical frequency-domain imaging," Opt. Express **11**(22), 2953–2963 (2003).
10. B. Cense, N. Nassif, T. C. Chen, M. C. Pierce, S. H. Yun, B. H. Park, B. E. Bouma, G. J. Tearney, and J. F. de Boer, "Ultrahigh-resolution high-speed retinal imaging using spectral-domain optical coherence tomography," Opt. Express **12**(11), 2435–2447 (2004).
11. A. F. Fercher, C. K. Hitzenberger, G. Kamp, and S. Y. El-Zaiat, "Measurements of intraocular distances by backscattering spectral interferometry," Opt. Commun. **117**(1-2), 43–48 (1995).
12. M. Wojtkowski, R. Leitgeb, A. Kowalczyk, T. Bajraszewski, and A. F. Fercher, "In vivo human retinal imaging by Fourier domain optical coherence tomography," J. Biomed. Opt. **7**(3), 457–463 (2002).
13. J. F. de Boer, B. Cense, B. H. Park, M. C. Pierce, G. J. Tearney, and B. E. Bouma, "Improved signal-to-noise ratio in spectral-domain compared with time-domain optical coherence tomography," Opt. Lett. **28**(21), 2067–2069 (2003).

#157957 - $15.00 USD Received 9 Nov 2011; revised 1 Dec 2011; accepted 2 Dec 2011; published 7 Dec 2011
(C) 2011 OSA

14. R. Leitgeb, C. K. Hitzenberger, and A. F. Fercher, "Performance of fourier domain vs. time domain optical coherence tomography," Opt. Express **11**(8), 889–894 (2003).
15. B. M. Hoeling, A. D. Fernandez, R. C. Haskell, E. Huang, W. R. Myers, D. C. Petersen, S. E. Ungersma, R. Y. Wang, M. E. Williams, and S. E. Fraser, "An optical coherence microscope for 3-dimensional imaging in developmental biology," Opt. Express **6**(7), 136–146 (2000).
16. F. Lexer, C. K. Hitzenberger, W. Drexler, S. Molebny, H. Sattmann, M. Sticker, and A. F. Fercher, "Dynamic coherent focus OCT with depth-independent transversal resolution," J. Mod. Opt. **46**, 541–553 (1999).
17. M. Pircher, E. Götzinger, and C. K. Hitzenberger, "Dynamic focus in optical coherence tomography for retinal imaging," J. Biomed. Opt. **11**(5), 054013 (2006).
18. L. An and R. K. Wang, "Use of a scanner to modulate spatial interferograms for in vivo full-range Fourier-domain optical coherence tomography," Opt. Lett. **32**(23), 3423–3425 (2007).
19. B. Baumann, M. Pircher, E. Götzinger, and C. K. Hitzenberger, "Full range complex spectral domain optical coherence tomography without additional phase shifters," Opt. Express **15**(20), 13375–13387 (2007).
20. A. F. Fercher, R. Leitgeb, C. K. Hitzenberger, H. Sattmann, and M. Wojtkowski, "Complex spectral interferometry OCT," Proc. SPIE **3564**, 173–178 (1998).
21. E. Götzinger, M. Pircher, R. A. Leitgeb, and C. K. Hitzenberger, "High speed full range complex spectral domain optical coherence tomography," Opt. Express **13**(2), 583–594 (2005).
22. R. A. Leitgeb, C. K. Hitzenberger, A. F. Fercher, and T. Bajraszewski, "Phase-shifting algorithm to achieve high-speed long-depth-range probing by frequency-domain optical coherence tomography," Opt. Lett. **28**(22), 2201–2203 (2003).
23. R. A. Leitgeb, R. Michaely, T. Lasser, and S. C. Sekhar, "Complex ambiguity-free Fourier domain optical coherence tomography through transverse scanning," Opt. Lett. **32**(23), 3453–3455 (2007).
24. M. Wojtkowski, A. Kowalczyk, R. Leitgeb, and A. F. Fercher, "Full range complex spectral optical coherence tomography technique in eye imaging," Opt. Lett. **27**(16), 1415–1417 (2002).
25. A. G. Podoleanu, J. A. Rogers, D. A. Jackson, and S. Dunne, "Three dimensional OCT images from retina and skin," Opt. Express **7**(9), 292–298 (2000).
26. K. Greco, M. Mujat, K. L. Galbally-Kinney, D. X. Hammer, R. D. Ferguson, N. Iftimia, P. Mulhall, P. Sharma, W. J. Kessler, and M. J. Pikal, "Accurate prediction of collapse temperature using optical coherence tomography (OCT) based freeze drying microscopy," submitted to J. Pharm. Sci.
27. A. A. Barresi, S. Ghio, D. Fissore, and R. Pisano, "Freeze drying of pharmaceutical excipients close to collapse temperature: influence of the process conditions on process time and product quality," Drying Technol. **27**(6), 805–816 (2009).
28. K. Chatterjee, E. Y. Shalaev, and R. Suryanarayanan, "Partially crystalline systems in lyophilization: II. Withstanding collapse at high primary drying temperatures and impact on protein activity recovery," J. Pharm. Sci. **94**(4), 809–820 (2005).
29. J. D. Colandene, L. M. Maldonado, A. T. Creagh, J. S. Vrettos, K. G. Goad, and T. M. Spitznagel, "Lyophilization cycle development for a high-concentration monoclonal antibody formulation lacking a crystalline bulking agent," J. Pharm. Sci. **96**(6), 1598–1608 (2007).
30. F. Fonseca, S. Passot, O. Cunin, and M. Marin, "Collapse temperature of freeze-dried Lactobacillus bulgaricus suspensions and protective media," Biotechnol. Prog. **20**(1), 229–238 (2004).
31. R. E. Johnson, M. E. Oldroyd, S. S. Ahmed, H. Gieseler, and L. M. Lewis, "Use of manometric temperature measurements (MTM) to characterize the freeze-drying behavior of amorphous protein formulations," J. Pharm. Sci. **99**(6), 2863–2873 (2010).
32. L. M. Lewis, R. E. Johnson, M. E. Oldroyd, S. S. Ahmed, L. Joseph, I. Saracovan, and S. Sinha, "Characterizing the freeze-drying behavior of model protein formulations," AAPS PharmSciTech **11**(4), 1580–1590 (2010).
33. D. E. Overcashier, T. W. Patapoff, and C. C. Hsu, "Lyophilization of protein formulations in vials: investigation of the relationship between resistance to vapor flow during primary drying and small-scale product collapse," J. Pharm. Sci. **88**(7), 688–695 (1999).
34. A. Parker, S. Rigby-Singleton, M. Perkins, D. Bates, D. Le Roux, C. J. Roberts, C. Madden-Smith, L. Lewis, D. L. Teagarden, R. E. Johnson, and S. S. Ahmed, "Determination of the influence of primary drying rates on the microscale structural attributes and physicochemical properties of protein containing lyophilized products," J. Pharm. Sci. **99**(11), 4616–4629 (2010).
35. S. C. Schneid, P. M. Stärtzel, P. Lettner, and H. Gieseler, "Robustness testing in pharmaceutical freeze-drying: Inter-relation of process conditions and product quality attributes studied for a vaccine formulation," Pharm. Dev. Technol. **16**(6), 583–590 (2011).
36. D. Q. Wang, J. M. Hey, and S. L. Nail, "Effect of collapse on the stability of freeze-dried recombinant factor VIII and α-amylase," J. Pharm. Sci. **93**(5), 1253–1263 (2004).

1. Introduction

The development of biological drugs often requires product formulations that must be lyophilized (freeze-dried) to produce stable products that can be stored in vials and reconstituted later for patient use. There are hundreds of biotechnology medicines and related products on the market and biotechnology drugs are the fastest growing segment of the

#157957 - $15.00 USD Received 9 Nov 2011; revised 1 Dec 2011; accepted 2 Dec 2011; published 7 Dec 2011
(C) 2011 OSA

pharmaceutical industry. Numerous biotechnology drugs were approved by the FDA and some of them are in late stage clinical trials [1]. Many new biotechnology drugs, including those used for the treatment of cancer are formulated and produced using the freeze-drying process. The most critical freeze-drying process design parameter is the temperature at which the product undergoes structural collapse during primary drying, which is called "collapse temperature" T_c [2]. Freeze-drying below T_c is necessary to ensure elegant appearance, low residual water content, and good storage stability and reconstitution characteristics. Therefore, accurate measurement of collapse is critical to freeze-drying process development. Since a 1°C temperature increase during primary drying can result in 13% reduction in primary drying time, it is essential to optimize the primary drying temperature at a value close to (but not exceeding) T_c [3]. This could reduce the production-scale freeze-drying process by several days, resulting in significant operating costs savings and accordingly, lower costs of biotechnology drugs.

T_c is currently estimated using two techniques, light transmission freeze-drying microscopy (LT-FDM) and/or differential scanning calorimetry (DSC). LT-FDM is performed using a high vacuum cold stage. A thin film of solution (1-2 µl) is frozen between two glass surfaces and subjected to vacuum. The temperature is slowly increased to bring about sublimation typically at a ramp rate of 1°C/min followed by an equilibration time. As the temperature rises, viscous flow results in changes to the structure of the freeze-dried solid which may result in collapse of the freeze-dried cake. Thin films may have different ice nucleation rates, crystallization tendencies for solutes, frozen product structures, and drying rates as compared to bulk products in vials. Thus, current LT-FDM does not always accurately estimate T_c for freeze-drying in a container of practical significance, a vial. Both theoretical and experimental evidence suggest that freeze-drying in a vial is sufficiently different than in a 2D sample used during LT-FDM that inefficient drying processes may be developed based upon LT-FDM. The difference in T_c determined using LT-FDM and that observed during freeze-drying in a vial is typically several degrees. This results in a 25% increase in drying time for every 2°C decrease in product processing temperature. Much larger discrepancies appear to occur in some protein formulations [4] and these differences may change as a function of formulation total solid content. A second technique, DSC, is used to determine the glass transition temperature of the maximally freeze concentrated solution (T_g') and is also used as an estimation of T_c [2]. T_g' is normally 1-3°C lower than T_c; however differences of 5-10°C have been reported [4]. Using T_g' as an estimate for T_c would result in a primary drying temperature that is lower than required, also unnecessarily extending the freeze-drying time.

Here we report on a new technique based on optical coherence tomography (OCT) to monitor changes in product structure while monitoring the product temperature to estimate T_c during freeze-drying in vials. This technique is intended to overcome the short-comings associated with determining T_c using DSC and LT-FDM by determining T_c in the same vial used during production operation. Moreover, the volumetric micron-level resolution and 3D imaging capabilities of OCT significantly enhance the current capabilities beyond the measurement of T_c to full exploration of the product response to temperature changes and imaging of structural changes and fine features of the freeze-drying process including ice nucleation and the freezing stage of lyophilization.

OCT was first demonstrated in 1991 [5]. Since then, numerous applications of OCT for both biomedical and material science applications have emerged. Medical applications of OCT are continuously evolving and OCT has revolutionized the technology of superficial and epithelial tissue imaging. Visualization of cells, microorganisms, hair, brain and the interior of arteries have been reported with depth and transversal resolution of 1-15 µm [6–9]. There are two main types of OCT, namely time-domain OCT (TDOCT) and Fourier-domain OCT (FDOCT). In TDOCT, each pixel within a 3D scan is measured individually and the scan volume is obtained by scanning in all three Cartesian directions sequentially. In FDOCT all

#157957 - $15.00 USD Received 9 Nov 2011; revised 1 Dec 2011; accepted 2 Dec 2011; published 7 Dec 2011
(C) 2011 OSA

pixels along an axial (depth) profile are measured simultaneously by Fourier transforming the spectrally resolved interference signal recorded either by a spectrometer (Spectral-domain OCT) [10–12] or by rapidly sweeping the source wavelength (Swept-source OCT) [9]. FDOCT has higher speed and an increased signal-to-noise ratio (SNR) compared to TDOCT [13,14]. There are, however, important limitations in FDOCT that still favor TDOCT as the option uniquely suited to certain applications. These limitations that are relevant for FDM are discussed below in the OCT design section.

2. The OCT system

The OCT system developed for the freeze-drying monitoring process is based on the time-domain approach. Although, the FD approach has proven to provide significant increase in both speed and signal-to-noise-ratio (SNR), it has some limitations, related to lateral resolution and depth sensitivity, which are critical for freeze dry monitoring. Here we discuss in more detail these important parameters.

Dynamic focusing. For Gaussian beams, the depth of focus and the beam waist (lateral resolution) are coupled. To achieve better lateral resolution one has to accept a short depth of focus. Conversely, if one requires a long depth of focus (2-3 mm), only a relatively poor lateral resolution (10-20 μm) can be achieved. Because the entire depth reflectivity profile is acquired simultaneously in FDOCT, the latter condition typically drives the design to prevent a large defocus along the axial profile (and concomitant worse lateral resolution and degraded image quality). This problem can be solved in TDOCT with dynamic focusing [15–17]. The in-focus region of the imaging beam and the coherence gate are scanned in depth simultaneously maintaining optimal focus and transverse resolution along the entire scan depth.

Roll-off. In FDOCT, the reflectivity profile exhibits an inherent roll-off with depth due to the finite spectrometer pixel size (typically 10-15 μm). The Fourier transform of the CCD pixel rectangular function results in a sinc function in the spatial (depth) domain that decreases with depth. The result is an inherent reduction of the detected signal with depth of the order of 5-15 dB/mm, depending upon spectrometer design and alignment. TDOCT, on the other hand, has a constant sensitivity with depth as there is no intensity roll-off.

Complex conjugate image. Fourier components outside the imaging window fold back into the imaging window in FDOCT. Sometimes their magnitude is small enough to not exceed the noise level, but in many cases, spurious reflections in the imaging system can bring significant unwanted artifacts into the imaging window making it difficult to distinguish between the real image and the complex conjugate image. These components do not appear in TDOCT allowing for the acquisition of images with reduced artifacts. Although there are methods to remove the complex conjugate image, they require additional hardware and signal processing techniques [18–24].

Depth penetration. The scattering properties of the sample reduce the detected signal with depth. Material science and biomedical applications typically involve highly scattering samples which limits the effective imaging depth. In addition to scattering, absorption also limits the effective imaging depth. Scattering decreases as the wavelength increases in the NIR but the absorption of water, the primary constituent of biological samples, increases. There are several low absorption windows at 800-900 nm and 1 μm and these spectral regions are preferred for applications where the sample has significant water content (like in ophthalmic applications where imaging is performed through more than 2 cm of water). In other applications involving dense scattering media, such as skin imaging however, the 1.3 μm wavelength is generally preferred as the reduction in scattering overcomes the increase of water absorption over the 1-2 mm imaging depth.

Because freeze-drying processes are extremely slow (durations of several hours to days) and the sample is stationary (as opposed to biological samples that often induce image motion artifacts), lateral resolution is more important than acquisition speed for this application. Also,

#157957 - $15.00 USD Received 9 Nov 2011; revised 1 Dec 2011; accepted 2 Dec 2011; published 7 Dec 2011
(C) 2011 OSA

the FDOCT SNR advantage was less critical because there are no inherent limitations to increasing the (source) signal level and SNR, as there are in, for example, ophthalmic applications with laser safety. Future experiments will be performed to ensure that the source intensity is not causing local heating within the frozen or freeze-dried cake. Based on the considerations described above, a TDOCT system with dynamic focusing at 1.3 μm was assembled for freeze-drying microscopy.

A schematic of the TDOCT system is shown in Fig. 1. The light from a broadband superluminescent diode (SLD, Inphenix, Livermore, CA; center wavelength - 1275 nm, bandwidth – 105 nm) was split by a 90/10 fiber splitter with 90% of light going to the sample arm and 10% going to the reference arm of the interferometer. An acousto-optic modulator (AOM, Brimrose Corporation of America, Baltimore, MD) was used in the reference arm to create a carrier frequency by phase modulating the optical signal. The delay line (Fig. 2 (b)) in the reference arm consisted of a collimator, a retroreflector, a prism, and two mirrors for folding the optical path in a compact space. The collimator was mounted on a translation stage to allow for adjusting the length of the reference arm to overlap the coherence gate with the microscope objective focal plane. The retroreflector was mounted on a motorized translation stage (Thorlabs, Newton, NJ) together with the microscope objective for z-scanning and dynamic focusing (Fig. 2 (b)). In this way the microscope objective was translated to move the focal plane along the axial direction as the retroreflector was moved the same distance to maintain the sample and the reference arms matched in length for interference. Optical circulators (AC Photonics, Santa Clara, CA) were used in the sample and reference arms for optimum light collection (Fig. 1 and Fig. 2 (b)) and two polarization controllers (General Photonics, Chino, CA) were used to improve the interference efficiency (Fig. 2 (b)). The light back-reflected from both the reference and the sample arm was recombined with a 50/50 fiber splitter/combiner and the interference signal was detected with a balanced detector (Thorlabs, Newton, NJ) which rejects the background and the common-mode signal noise.

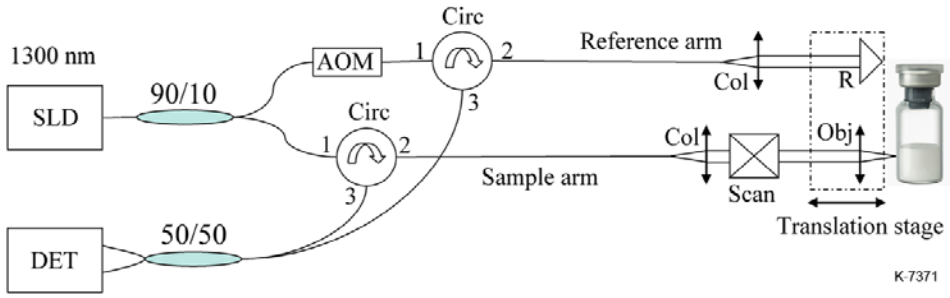

Fig. 1. TDOCT setup. SLD – 1300 nm superluminescent diode; DET—balance detector; AOM—acousto-optic modulator; Circ—circulator; Col—collimator; R—retroreflector; Obj—microscope objective; Scan—scanning optics; 90/10 and 50/50 fiber beamsplitters.

Special attention was given to the dispersion mismatch between the sample and the reference arms. The mismatch was mainly due to the AOM which consists of two 1 cm long AMTIR crystals (Amorphous Materials Inc, Garland TX) with a refractive index of 2.55 at 1.3 μm. Dispersion (variation of refractive index with wavelength) mismatch between reference and sample arms causes broadening of the coherence peak and therefore a loss of axial resolution. To compensate for this dispersion mismatch a 1 cm thick AMTIR window was inserted in the free-space region of the sample arm. The light transmitted to and from the sample passed twice through the 1 cm AMTIR window compensating for the 2 cm of AMTIR in the AOM.

The fiber optic components of the interferometer including the polarization controllers, the AOM, and the detector were placed on an 8”x12” breadboard (Fig. 2 (b)) that was mounted on four posts above the scanning optics. The scanning optics and the delay line occupied

#157957 - $15.00 USD Received 9 Nov 2011; revised 1 Dec 2011; accepted 2 Dec 2011; published 7 Dec 2011
(C) 2011 OSA

approximately one half of a 12”x18” breadboard (Fig. 2 (a) and Fig. 3 (b)); the other half of the breadboard was used to mount the single-vial freeze dryer (not shown here).

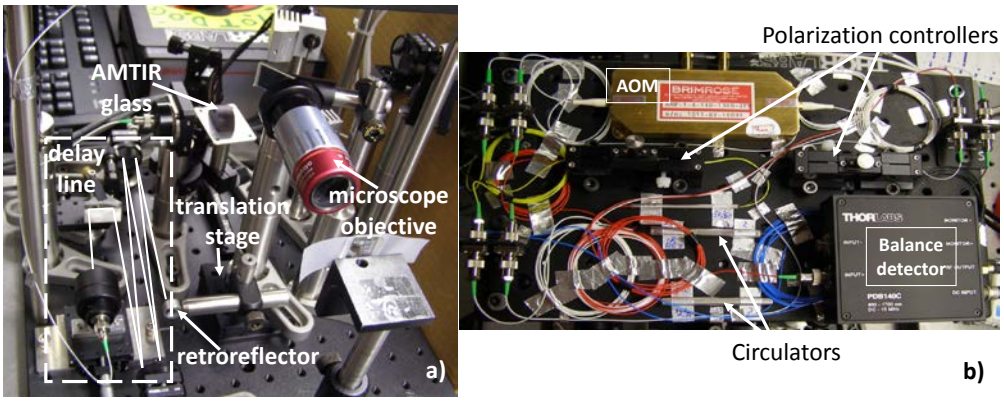

Fig. 2. (a) Fiber-optic based interferometer and (b) the scanning optics.

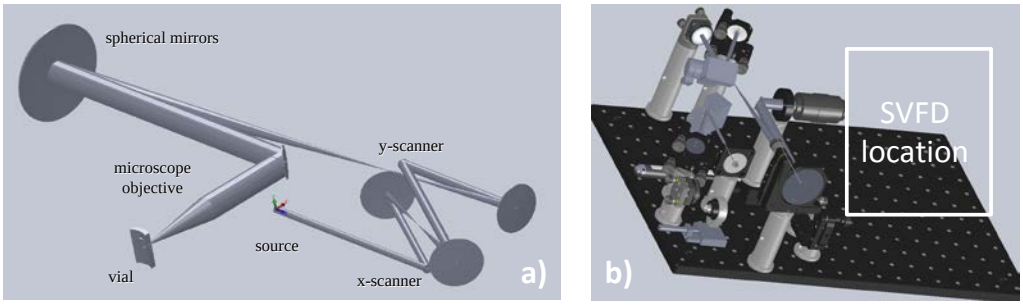

Fig. 3. (a) Zemax optical design and (b) SolidWorks mechanical design.

The scanning optics (Fig. 3) consisted of a collimator, a microscope objective (5x Plan Apo NIR Infinity-Corrected Objective, Mitutoyo, Japan), two galvanometers for *x*-*y* scanning (Thorlabs, Newton, NJ), and five mirrors for folding the optical path. Four of the mirrors were spherical and had two functions: first, they formed two stages of magnification to maintain the laser beam diameter small (2-5 mm) on the galvanometers’ mirrors and to expand it to 10 mm diameter to fill up the microscope objective pupil; and second, they ensured that the galvanometer mirrors were relayed to the objective pupil such that the scanning beam had a pivoting point at the objective entrance pupil. A large beam diameter at the objective pupil was needed to ensure the best performance of the objective (the smallest spot on the sample). The pupil beam diameter is inversely proportional to the beam waist in the focal plane, which represents the lateral resolution of the imaging system. A Zemax optical design was performed to optimize the performance of the optical system and a SolidWorks mechanical design was developed to guide the fabrication of the system (Fig. 3).

The signal from the balanced detector was acquired by a high-speed digitizer board (National Instruments, Austin, TX) that also performed data processing. A LabVIEW interface was developed to control the OCT hardware, data acquisition and processing, real-time image display and data storage. This included control of the galvanometer scanners for *x*-*y* scanning and of the motorized translation stage for *z*-scanning and dynamic focusing, synchronization of the galvanometers with the digitizer for data acquisition, and synchronization with the software controlling the single-vial freeze-dryer. An additional data-acquisition board (National Instruments, Austin, TX) transferred the galvanometer signals and the synchronization signals to the freeze-drying hardware.

#157957 - $15.00 USD Received 9 Nov 2011; revised 1 Dec 2011; accepted 2 Dec 2011; published 7 Dec 2011
(C) 2011 OSA

The OCT system was configured to include several scan modes: **1)** a single frame *x*-*z* scan mode was used for sample alignment after the vial was introduced in the freeze-dryer chamber to bring the vial-product interface (inner vial surface) close to the side of the imaging window. This scan mode allowed for the determination of the optimum axial (*z*) limits of the 3D scan volume. **2)** A second scan mode allowed for a single 3D scan volume in *en-face* mode (*x*-*y* first and then step axially). **3)** The standard measurement scan mode allowed for scanning 3D volumes synchronized with the freeze-drying temperature control. The number of temperature steps (and therefore of the 3D volumes to be acquired) was set first, and then after each OCT volume scan a digital signal was sent to the freeze-dryer hardware control to step and hold the dryer shelf temperature at the next value. The OCT software waited until the freeze-dryer hardware control returned a signal indicating that the required temperature had been reached and then it continued with the next volume scan.

OCT scan settings. The scanning coordinate system had the *x* and *y* axes in a plane perpendicular to the incident laser beam (*en-face* cross-section) and the *z* axis along the incident beam (depth into the sample). The scanning protocol was defined by: *x*-axis – fast scanning, *y*-axis – slow scanning, and *z*-axis – the slowest scanning [25]. This approach relaxed the requirements on the speed of the dynamic focusing (along the *z* axis). In this manner, depth scanning and dynamic focusing could be implemented using a relatively slow motorized translation stage.

One *x*-*y* frames took 0.75 s for scanning and 0.67 s for processing for a total of 1.42 s per frame and 282 s per volume.

Lateral resolution. The theoretical lateral resolution ($4\lambda f/\pi D$) given by the beam diameter D = 10 mm, focal length of the objective f = 40 mm and wavelength λ = 1.275 μm is 6.5 μm. The depth of focus ($8\lambda/\pi*(f/D)^2$) was estimated at 52 μm. The lateral resolution was measured using the standard USAF 1951 calibration target. Group 7 element 2 could be resolved giving a lateral resolution of 6.9 μm.

Axial resolution. The theoretical coherence length ($2\ln 2\lambda^2/\pi\Delta\lambda$) given by the central wavelength λ = 1.275 μm and the bandwidth $\Delta\lambda$ = 105 nm (manufacturer specifications) is 6.8 μm in air. However, the measured spectrum had a bandwidth of 65 nm giving a coherence length of 11 μm in air. Spectral narrowing may have been caused by the limited bandwidth of the optical components including fiber couplers, circulators, and most significantly, the AOM. The coherence length was measured by analyzing the depth profile of a mirror (full width at half maximum of the intensity coherence peak). The measured value of the coherence length was 13 μm. The axial resolution is defined as half of the coherence length and therefore, the measured value was 6.5 μm in air and 4.7 μm in the sample assuming an average refractive index of the sample or 1.38 (slightly larger than that of water due to the pharmaceutical formulation which could vary from sample to sample).

3. The single vial freeze dryer

A bench top single-vial freeze dryer (SVFD) was also designed and fabricated for this study. The main components of the freeze-dryer system were the: drying chamber, product shelf, heat transfer system, cooling system, condenser, vacuum pumping system, and process control instrumentation. One side of the SVFD contained an AR-coated glass window for OCT measurements. Detailed description of the SVFD and of the measurement results for various pharmaceutically representative formulations were presented elsewhere [26].

4. Results

A preliminary test of the OCT-FDM system was performed by studying the collapse of a 5% sucrose solution in a 5 ml vial (0.75 ml of solution with about 4.5 mm product height in the vial). The shelf temperature was lowered from room temperature to −45°C and held for 45 minutes to freeze the product and then it was raised to −40°C for 5 minutes. Vacuum was pulled on the SVFD and the temperature was raised by 2°C every 6 minutes to −10°C to

#157957 - $15.00 USD Received 9 Nov 2011; revised 1 Dec 2011; accepted 2 Dec 2011; published 7 Dec 2011
(C) 2011 OSA

facilitate sublimation. OCT measurements at each temperature step were completed in ~5 minutes.

The frozen solution and the freeze-dried solid are visible using OCT-FDM as shown in Fig. 4. The reported temperatures are from the thermocouple located in the bottom center of the vial. At –28.9°C the solid structure begins to display gaps in the *x-y* cross section (*en face* view). In the *z-y* view the solid appears to be separating from the vial wall. In the video of the OCT-FDM (Media 1) for this formulation one can see complete separation of the freeze dried solid from the frozen solid, signifying complete collapse of the formulation. In Fig. 4 (a and b), Media 1 shows the collapse in the *x-y* direction while Media 2 shows the collapse in the *z-y* direction. The onset of collapse was determined to be –28.9°C, the temperature at which gaps in the dried cake were first observed. LT-FDM measurements of the same formulations were performed and the onset of collapse was observed at –32°C. Therefore, the T_c observed using OCT-FDM is ~3°C higher than measured using LT-FDM. This difference is consistent with the expected difference between freeze-drying in a vial and results obtained with the LT-FDM method [2]. A lyophilization cycle based on the T_c found by OCT-FDM rather than LT-FDM would result in a significant reduction in the primary drying time for this formulation (35-40% shorter).

The OCT system acquires data in a 3D volume with a scan size – 0.75 mm / 4 mm / 1.5 mm (*x/y/z*). To demonstrate the 3D visualization capability of OCT-FDM, Amira image processing software (Visage Imaging, Inc.) was used to compile a 3D display of the OCT data. The movie linked to Fig. 4 (c) shows the 4D structural changes (time/temperature evolution of the 3D representation of the product) for 5% sucrose as described above. The movie indicates the shelf and product temperature for each frame (3D scan) and ends with a rotation of the 3D structure for better visualization of the collapsed structure. The fixed surface in the sucrose movie is the vial inner interface.

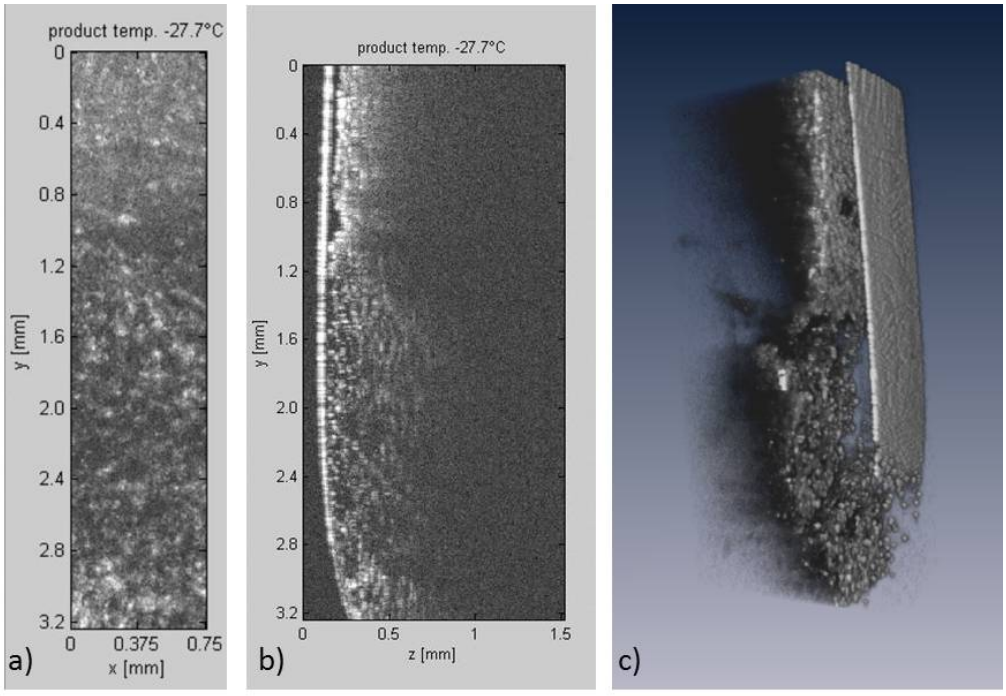

Fig. 4. 2D cross-sections of 5% sucrose freeze-dried in a vial, (a)x-y view (Media 1), and (b) z-y view (Media 2); (c) time evolution of the freeze-drying process in a 3D representation (Media 3).

#157957 - $15.00 USD Received 9 Nov 2011; revised 1 Dec 2011; accepted 2 Dec 2011; published 7 Dec 2011
(C) 2011 OSA

5. Conclusion

A new type of freeze-drying microscope based on time-domain OCT was developed and demonstrated for the first time to measure T_c of product formulations freeze-dried in standard pharmaceutical vials. The OCT imaging system provided the means to measure a T_c that was predictive of freeze-drying characteristics of a batch of vials, as performed in a realistic manufacturing environment. This imaging tool has enormous advantages, particularly with formulations that can be freeze-dried above the T_c determined with LT-FDM without loss of product quality. Other investigators have reported freeze-drying near or above the T_c as measured by LT-FDM with no evidence of macroscopic collapse of freeze-dried cake [27–36]. Prior to our application of OCT to freeze-drying microscopy, T_c measured for formulations using DSC or LT-FDM could not be assumed to be accurately predictive of freeze-drying in a vial or other large container of commercial significance. The T_c measured by OCT-FDM provides quantitative justification for freeze-drying above T_c as measured by LT-FDM. OCT-FDM provides an upper limit to the temperature at which a lyophilization cycle may be run without macroscopic product collapse. These data will help to reduce the time for primary drying and increase process efficiency for freeze dried products with more accuracy than current methods (LT-FDM, DSC). Literature data [4] suggest that the difference between collapse measured by LT-FDM and collapse that occurs in vials may be particularly large for protein formulations. As the importance of therapeutic proteins continues to grow, and the cost savings potentially resulting from "biosimilars" (i.e., "generic" therapeutic proteins) continues to receive emphasis from both Congress and the FDA, the benefits of OCT-FDM for product microstructure visualization and manufacturing process design will also assume greater importance.

Acknowledgments

The project described was supported by the National Institute of Biomedical Imaging and Bioengineering Award Number R43EB010317. The content is solely the responsibility of the author(s) and does not necessarily represent the official views of the National Institute of Biomedical Imaging and Bioengineering or the National Institutes of Health.

#157957 - $15.00 USD Received 9 Nov 2011; revised 1 Dec 2011; accepted 2 Dec 2011; published 7 Dec 2011
(C) 2011 OSA